Chemical Science

ROYAL SOCIETY OF CHEMISTRY

EDGE ARTICLE

View Article Online
View Journal | View Issue



Cite this: *Chem. Sci.*, 2024, **15**, 18443

All publication charges for this article have been paid for by the Royal Society of Chemistry

Received 17th January 2024
Accepted 28th September 2024

DOI: 10.1039/d4sc00402g

rsc.li/chemical-science



# Visualization of membrane localization and the functional state of $CB_2R$ pools using matched agonist and inverse agonist probe pairs†

M. Wąsińska-Kałwa,‡[a] A. Omran,‡[a] L. Mach,‡[a] L. Scipioni, ‡[cj] J. Bouma,[b] X. Li,[de] S. Radetzki,[a] Y. Mostinski,[a] M. Schippers,[f] T. Gazzi,[a] C. van der Horst,[b] B. Brennecke,[a] A. Hanske,[a] Y. Kolomeets,[a] W. Guba,[f] D. Sykes,[gh] J. P. von Kries,[a] J. Broichhagen, [a] T. Hua,[de] D. Veprintsev,[gh] L. H. Heitman,[b] S. Oddi, *[ij] M. Maccarrone, *[cj] U. Grether*[f] and M. Nazare *[a]

The diversity of physiological roles of the endocannabinoid system has turned it into an attractive yet elusive therapeutic target. However, chemical probes with various functionalities could pave the way for a better understanding of the endocannabinoid system at the cellular level. Notably, inverse agonists of $CB_2R$ – a key receptor of the endocannabinoid system – lagged behind despite the evidence regarding the therapeutic potential of its antagonism. Herein, we report a matched fluorescent probe pair based on a common chemotype to address and visualize both the active and inactive states of $CB_2R$, selectively. Alongside extensive cross-validation by flow cytometry, time-lapse confocal microscopy, and super-resolution microscopy, we successfully visualize the intracellular localization of $CB_2R$ pools in live cells. The synthetic simplicity, together with the high $CB_2R$-selectivity and specificity of our probes, turns them into valuable tools in chemical biology and drug development that can benefit the clinical translatability of $CB_2R$-based drugs.

## Introduction

The endocannabinoid system (ECS) is a complex lipid-based signalling network involved in a wide variety of physiological and cognitive processes such as pain regulation, immune response, appetite control, learning and memory formation, cardiovascular regulation, and addictive-like behaviour.[1] The ECS consists of two cannabinoid receptor subtypes ($CB_1R$ and $CB_2R$) that belong to the class A G protein-coupled receptor (GPCR) family. Arachidonoylethanolamide (AEA) and 2-arachidonoylglycerol (2-AG) are the endogenous ligands of both $CB_1R$ and $CB_2R$.[2] Regardless of their high homology, the key difference between the two receptors is their distribution.[3] $CB_1R$ is predominantly expressed in the central nervous system with the highest density in the cerebellum, hippocampus, and cerebral cortex,[4–6] while $CB_2R$ is more abundant in peripheral organs, such as the spleen and tonsils, and is mainly expressed in cells associated with the immune system.[3] It has been shown that expression of $CB_2R$ is strongly upregulated under pathological conditions such as cancer,[7,8] immunological disorders,[9] inflammation, neurodegenerative diseases,[10,11] and drug abuse.[12] Therefore, modulating $CB_2R$ activation will be a valuable therapeutic approach for several diseases including inflammation, autoimmune and metabolic disorders, chronic pain, multiple sclerosis and cancer. For example, agonist-mediated activation of $CB_2R$ was previously shown to be beneficial for neuroprotection in chronic neurodegenerative disorders such as Huntington's and Alzheimer's diseases.[13] Conversely, inactivation of $CB_2R$ *via* an inverse agonist/antagonist was found to have therapeutic potential for treatment of various diseases associated with neuroinflammation

[a]*Leibniz-Forschungsinstitut für Molekulare Pharmakologie FMP, Campus Berlin-Buch, 13125 Berlin, Germany. E-mail: nazare@fmp-berlin.de*

[b]*Division of Drug Discovery and Safety, Leiden Academic Centre for Drug Research, Leiden University, 2333 CC, Leiden, The Netherlands*

[c]*Department of Biotechnological and Applied Clinical Sciences, University of L'Aquila, 67100 L'Aquila, Italy. E-mail: mauro.maccarrone@univaq.it*

[d]*iHuman Institute, ShanghaiTech University, Shanghai 201210, China*

[e]*School of Life Science and Technology, ShanghaiTech University, Shanghai 201210, China*

[f]*Roche Pharma Research & Early Development, Roche Innovation Center Basel, F. Hoffmann-La Roche Ltd, 4070 Basel, Switzerland. E-mail: uwe.grether@roche.com*

[g]*Division of Physiology, Pharmacology & Neuroscience, School of Life Sciences, University of Nottingham, Nottingham, NG7 2UH, UK*

[h]*Centre of Membrane Proteins and Receptors (COMPARE), University of Birmingham, University of Nottingham, Midlands, UK*

[i]*Department of Veterinary Medicine, University of Teramo, Via R. Balzarini 1, 64100 Teramo, Italy. E-mail: soddi@unite.it*

[j]*European Center for Brain Research/Institute for Research and Health Care (IRCCS) Santa Lucia Foundation, via del Fosso di Fiorano 64, 00143 Rome, Italy*

† Electronic supplementary information (ESI) available. See DOI: https://doi.org/10.1039/d4sc00402g

‡ These authors contributed equally to this work.

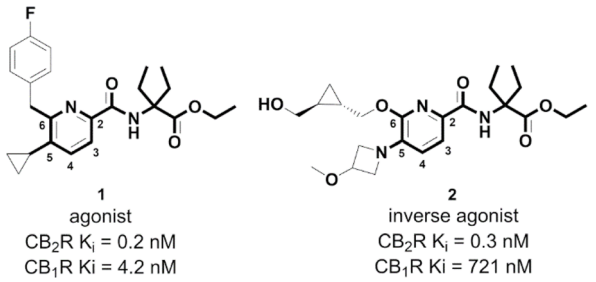


Fig. 1 Chemical structures of $CB_2R$ agonist **1** and inverse agonist **2** sharing a 5- and 6-substituted picolinamide core.

and the immune system.[14,15] Due to different expression patterns of $CB_2R$ and $CB_1R$, as well as their distinct functions, the selective activation or deactivation of $CB_2R$ does not involve undesired psychotropic responses which is considered a major therapeutic advantage and makes it a more attractive target compared to $CB_1R$. However, despite its great potential, no $CB_2R$-selective drug has made its way to the market to date, as clinical translatability from preclinical models deduced from different species is currently challenging.[14] This is largely attributed to the highly inducible nature and complexity of $CB_2R$ signalling pathways at the cellular level and the unclear understanding of its expression, localization and function.[16] For

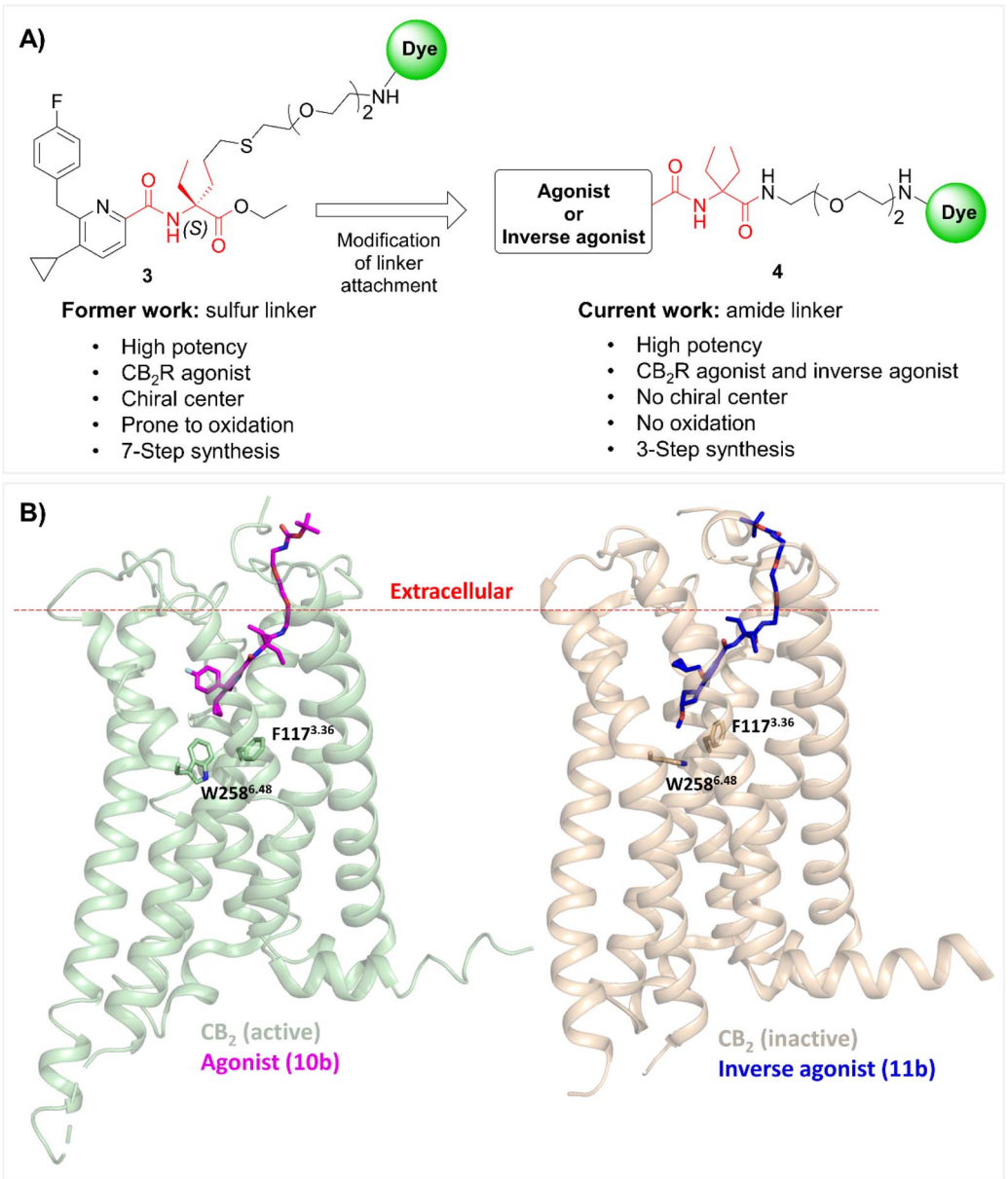


Fig. 2 (A) Modification of linker attachment from previous work (compound **3**; sulfur linker) led to the discovery of a new versatile exit vector (compound **4**; amide linker), and the diethylglycine moiety as the centerpiece hub in red. (B) Docking poses of compounds **10b** (magenta sticks) and **11b** (blue sticks) within active (green; PDB: 6KPF) and inactive (orange; PDB: 5ZTY) states of $CB_2R$, respectively. The red dashed line indicates the approximate boundary of the lipid bilayers. For a detailed description of the docking studies see ESI, S3.†

example, a number of studies indicate that the cellular responses associated with $CB_2R$ activation are not only limited to plasmalemmal receptors but also to the intracellular pools.[17–19] The absence of $CB_2R$-specific monoclonal antibodies, which are important tools for obtaining expression data at a cellular or tissue level, is further aggravating this situation.

Recent $CB_2R$-selective agonist fluorescent probes[20–22] could partially fill these gaps by addressing the activated state and providing information on $CB_2R$ localization, expression, target engagement, pharmacokinetics and dynamics in real-time; the scarcity of labeled $CB_2R$-selective inverse agonist probes has resulted in a lack of information on the distribution of intra- and extracellular $CB_2R$ pools in the inactivated state. There are only a limited number of reports about inverse agonist fluorescent probes labeling $CB_2R$. For example, the chromenopyrazole-based inverse agonist probe was originally generated from an agonist but upon attachment of the Cy5 fluorescent dye, the functionality was altered.[23] The surface receptors of $CB_2R$ expressing HEK-293 cells were labeled *via* the aforementioned probe.[23] Another example is **NIR-mbc94**, an analogue of selective inverse agonist **SR144528**, which has been shown to be an imaging agent for the unbiased high-throughput screening of compounds interacting with $CB_2R$ as a therapeutic target.[24] Despite the wide range of applications and a high demand for $CB_2R$ inverse agonist probes, no versatile probe platform with diverse fluorophores is available so far.

We have previously reported a high-affinity, cell-permeable fluorescent $CB_2R$ probe **3** based on a reverse-design approach using a preclinically validated drug-derived $CB_2R$ agonist **1** (Fig. 1 and 2).[20] The probe successfully detected $CB_2R$ in several *in vitro* and *in vivo* settings across species. For example, **3** was also recently used to visualize the high expression levels of $CB_2R$ in primary neonatal microglia isolated from wild-type and Tg2576 mice, the latter being used as an Alzheimer's Disease (AD) model.[25]

However, for any chemical probe approach, it is desirable to have access to a matched molecular pair of agonist and inverse agonist with high structural similarity which are correspondingly labeled. Such chemical probes are most suitable to address distinct mechanisms of action, *e.g.* by distinguishing the activated or resting state of the receptor or allowing differential analysis of agonist-stimulated internalization of the receptor, while excluding the cellular phenotype.

With the goal of expanding the scope of our probe platform and addressing both active and inactive states of the receptor, we designed a matched molecular pair of $CB_2R$ agonist and antagonist fluorescent probes derived from highly similar chemotypes of advanced preclinical $CB_2R$ agonist **1** (ref. 26) and inverse agonist **2** (ref. 27) drug candidates (Fig. 1). In addition, we were able to attach a variety of fluorescent dyes leading to $CB_2R$ probes that span a broad range of physicochemical properties. At last, varying combinations of agonist and antagonist with cell-permeable (*e.g.* TAMRA) or impermeable (*e.g.* Alexa488) fluorophores gave us access to a valuable toolbox suitable for detecting extra- and intracellular receptor pools. To explore the spatial–temporal dynamics of $CB_2R$, we employed these novel probes to investigate the expression and subcellular localization of the active and inactive states of $CB_2R$ in living cells, utilizing super-resolution confocal imaging techniques.

## Results and discussion

### Probe design and molecular modelling

Our previous probes were derived from a drug-like $CB_2R$ agonist bearing a 5,6-substituted picolinamide **1** (Fig. 1). Interestingly, it was shown that different substitutions at the 5- and 6-positions of picolinamide could alter the functionality of the ligand while maintaining high $CB_2R$ affinity.[27,28] For example, the replacement of the cyclopropyl moiety at position 5 of agonist **1** with 3-methoxy-azetidine alters the functionality from agonism to inverse agonism (**2**). This substitution causes a flip of the side chain of the toggle switch residue $W258^{6.48}$ (Ballesteros–Weinstein numbering in superscript, Fig. 2B).[29] Besides the 5,6-substituents, both ethyl side chains are involved in favorable van der Waals interactions with surrounding phenylalanine side chains F91, F94, and F106.

The drug-derived inverse agonist **2** possessing an exceptional selectivity profile ($CB_2R$ $K_i$ = 0.3 nM; $CB_1R$ $K_i$ = 721 nM; a selectivity factor of 1403 over $CB_1R$) was an ideal starting point for generating a matched agonist and inverse agonist-based probe pair with a 5,6-substituted picolinamide core in common.[28,30,31]

The first and the most critical step in probe design is the identification of a suitable attachment point between the recognition element and the reporter unit, *i.e.* the ligand and fluorescent dye, respectively. In most cases, the recognition element and the fluorescent dye are distanced using a suitable linker, which allows the dye to access the extracellular space without compromising overall binding affinity.[32] Previously, we introduced a hybrid of thio- and polyether chains to one of the ethyl groups of the diethylglycine moiety as the centerpiece hub (**3**, Fig. 2A). Even though our previous probes showed highly consistent interspecies affinity and potency for both human and mouse $CB_2R$, the presence of the sulfur atom in the linker posed a possible experimental imponderability in some of the advanced settings, as sulfur might be prone to oxidation.[20,33] Therefore, with the goal of improving the physicochemical properties and simplifying the synthetic strategy, SAR studies were performed to investigate alternative sites for linker attachment at the diethylglycine centerpiece hub. For this, we used the ester functionality which after substitution by an amide moiety served as an attachment point. This design approach has the advantage that no chiral center is present and the synthesis route is greatly simplified compared to our previous probes (**4**, Fig. 2A).

Docking experiments were conducted to estimate the required linker length to reach out into the extracellular space and support linkerology studies. In Fig. 2B the best docking poses for agonist (**10b**) and inverse agonist (**11b**) pharmacophores, respectively, are depicted. For both ligands, the proper range of polyethylene glycol PEG chains to access the extracellular space for insertion of the fluorescent dye was estimated to be $n = 2$.

## Chemistry

The synthetic pathway to access the Boc-protected intermediates and target fluorescent probes bearing various dyes is outlined in Scheme 1. Fmoc-protected diethylglycine **5** was used as the centerpiece unit to connect the 5,6-substituted picolinamide recognition elements to the desired linker. In order to elaborate the optimal linker length for dye attachment, compound **5** was functionalized with a series of linkers **6a–d** with different lengths under HATU-mediated amide coupling conditions. Fmoc-protecting group removal of compounds **7a–d** using DBU was followed by coupling to agonist **8** or inverse agonist **9** precursors *in situ* to afford Boc-protected congeners with matched chemotypes (**10a–d** and **11a–d**). Compounds **8** (ref. 20) and **9** (ref. 31) were synthesized according to literature protocols. The final step was to conjugate a variety of broadly used fluorophores such as 5/6-TAMRA, SiR, 5/6-Alexa488 and Alexa647 to the selected intermediates (**10b** and **11b**) with a linker length of $n = 2$, which turned out to be optimal in subsequent SAR studies. For this purpose, the Boc-protecting group of **10b** or **11b** was first cleaved using TFA. Subsequently, the resulting free amines were coupled with the desired fluorescent dyes either under suitable amide coupling conditions to furnish probes **12–15** and **17–18**. Compound **16** was synthesized *via* a variation of the aforementioned synthetic route starting with coupling of 5/6-TAMRA-COOH to Boc-deprotected **7b** followed by another amide coupling reaction to **9** using HATU as the coupling reagent (ESI, S32†).

## Evaluation of the appropriate linker length

To identify the optimal linker length, binding affinities of unlabeled precursors **10a–d** and **11a–d** were measured *via* a competitive radioligand binding assay on CHO membranes stably expressing $hCB_1R$ or $hCB_2R$ (Table 1).

For both agonist and inverse agonist chemotypes, the PEG chain with $n = 2$ (**10b** and **11b**, respectively) showed the highest affinity and selectivity for $CB_2R$ and was therefore chosen as the optimal linker length. The observed trend confirmed the predictions based on our docking studies (Fig. 2B). To assess whether the attachment of the linker affects receptor function, the efficacy of selected precursors was determined in a cAMP assay (Table 1). Notably, **10b** and **11b** preserved partial agonist and inverse agonist activity, respectively, with high potency

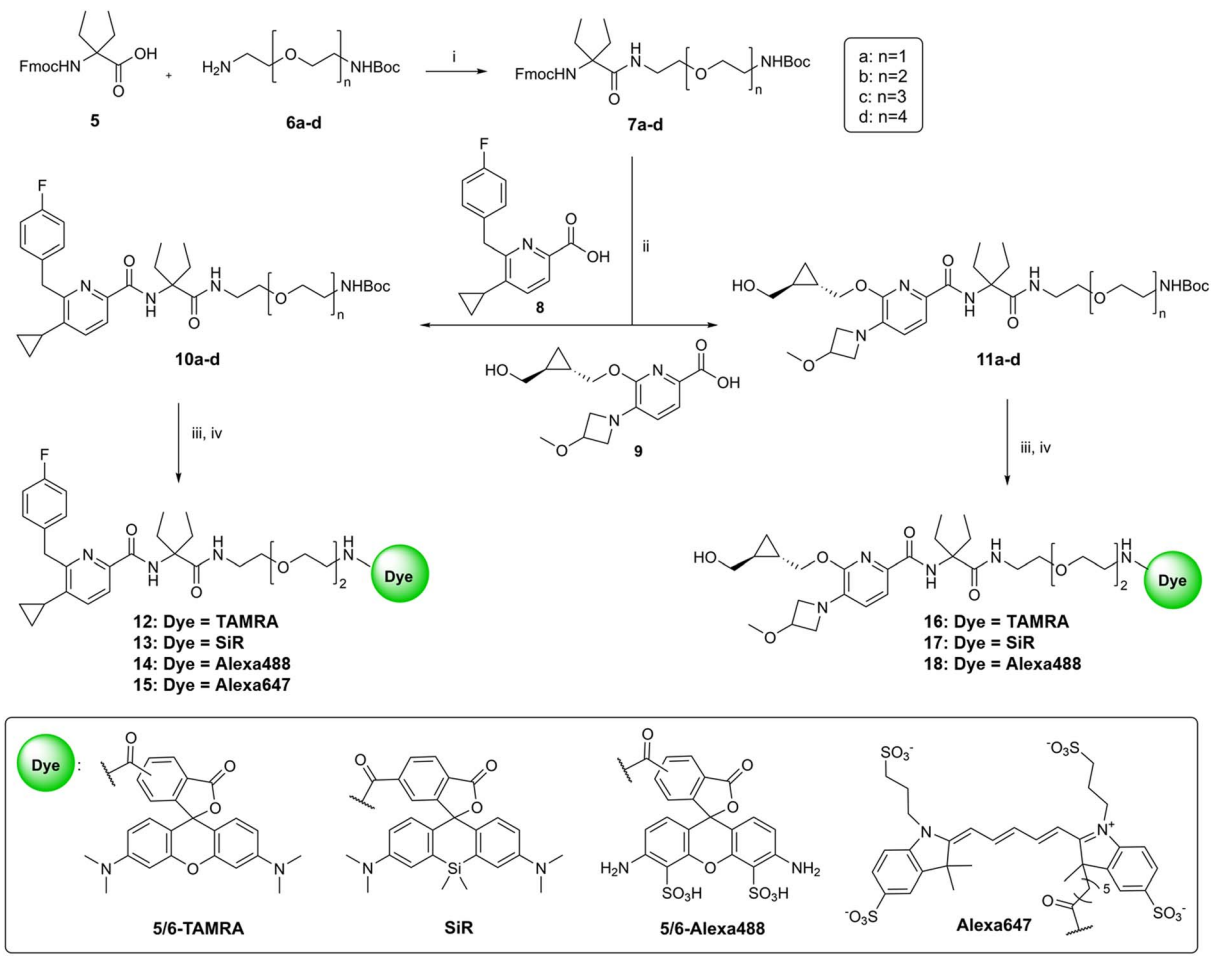


Scheme 1 Synthesis of fluorescent probes. Reagents and conditions: (i) HATU, DIPEA, DMF, rt, 1 h; (ii) (1) DBU, HOAt, DMF, rt, 20 min; (2) **8** or **9**, HATU, DIPEA, DMF, rt, 10 h; (iii) TFA (9 equiv.), $CH_2Cl_2$, 0 °C to rt, 3 h; (iv) for compounds **13**, **15**, **17** and **18**: HATU, dye, DIPEA, DMF, rt, 10 h; for compound **12**: EDC·HCl, HOAT, dye, DIPEA, DMF, rt, 10 h; for compound **14**: dye, DIPEA, DMF, rt, 10 h; for compound **16**: see the ESI.†

Table 1 Binding affinities and potency of the Boc-protected intermediates

| | | $K_i$[a] (nM) | | | | | | |
|---|---|---|---|---|---|---|---|---|
| Cmpd | Linker length | $hCB_1R$ | $hCB_2R$ | Selectivity[b] | $EC_{50}$ or $IC_{50}$[c] (nM) | $E_{max}$[d] (%) | Function | Parent cmpd |
| **1** | n.a. | 4.2 | 0.2 | 21 | 6.5 | 102 | Agonist | n.a. |
| **2** | n.a. | 721 | 0.3 | 1403 | 4.4 | −130 | Inverse agonist | n.a. |
| **10a** | $n = 1$ | 836 | 28 | 30 | n.d. | n.d. | n.d. | 1 |
| **10b** | $n = 2$ | 466 | 6 | 78 | 49 | 83 | Agonist | 1 |
| **10c** | $n = 3$ | 748 | 63 | 12 | n.d. | n.d. | n.d. | 1 |
| **10d** | $n = 4$ | 1472 | 144 | 10 | n.d. | n.d. | n.d. | 1 |
| **11a** | $n = 1$ | >10 000 | 2061 | >4 | n.d. | n.d. | n.d. | 2 |
| **11b** | $n = 2$ | >10 000 | 106 | >94 | 88 | −63 | Inverse agonist | 2 |
| **11c** | $n = 3$ | >10 000 | >10 000 | n.a. | n.d. | n.d. | n.d. | 2 |

[a] $K_i$ (nM) values obtained from [$^3$H]CP55940 displacement assays on CHO membranes stably expressing $hCB_1R$ or $hCB_2R$. Values are means of at least three independent experiments performed in duplicate. For details, see the ESI. [b] Selectivity was determined by calculating the ratio of $K_i$ ($CB_1R$)/$K_i$ ($CB_2R$). [c] The potency ($EC_{50}$ or $IC_{50}$) of the selected compounds was measured using cells stably expressing $hCB_2R$ in homogeneous time-resolved fluorescence (HTRF) cAMP assay. The data are the means of four independent experiments performed in technical replicates. [d] Maximum effect ($E_{max}$ in %) was normalized to reference full agonist **APD371**. n.a. is not applicable. n.d. is not determined.

($CB_2R$ cAMP $EC_{50}$ = 49 nM for **10b** and $IC_{50}$ = 88 nM for **11b**, respectively).

### Pharmacological characterization of fluorescent probes 12–18

Compared to their unlabeled congeners, the binding affinity of the fluorescent probes **12–18** indicated fluorescent dye dependency which was not unexpected as the structural nature of the fluorophore alters the membrane interactions of the constructs. Overall, we observed a certain drop in affinity for all dye-bearing probes, consistent with previous results.[20,21,34] This decrease is believed to mainly originate from additional configurational and steric penalties due to conjugation.[35] However, most of the probes retained high affinity and selectivity for $CB_2R$ (ESI, Table S-2†).

In functional studies (Table 2), probes **13** and **15** showed full agonism with potencies ($EC_{50}$) of approximately 525 nM, while **12** and **14** showed partial agonism with higher potencies ($EC_{50}$) of approximately 80 nM. As anticipated, the functional mode of action of probes **16–18** fully retained their inverse agonism with $IC_{50}$ values in the range of 114–262 nM (Table 2 and Fig. 3).

To assess the specificity of the probes and scout for putative off-targets, TAMRA-probe pairs **12** and **16** were screened against a customized panel of 50 representative receptors and enzymes.[37] Both probes were devoid of any relevant off-target interactions thus confirming their suitability for specific $CB_2R$ detection studies (ESI, Table S-1†). Furthermore, kinetic binding characterization of agonist **12** and inverse agonist **16** using HEK293-$hCB_2R$ cell membranes revealed fast association and appropriate residence time (ESI, Fig. S-8†).

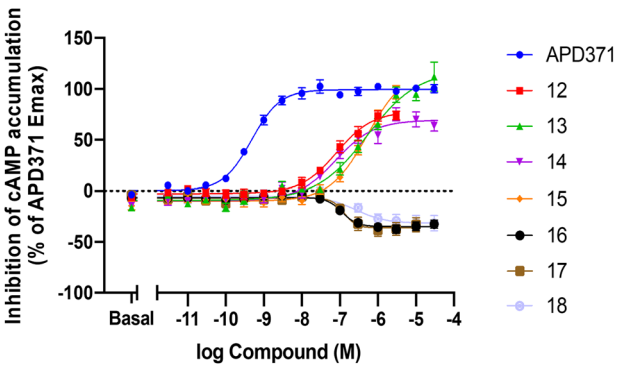


Fig. 3 Inhibition of cAMP accumulation on $hCB_2R$ was determined with a (HTRF) cAMP assay. The maximum effect ($E_{max}$ in %) was normalized to reference full agonist **APD371**.

Table 2 $hCB_2R$ potency and predicted log $D_{7.4}$ of fluorescent probes **12–18**

| Cmpd | $EC_{50}$ or $IC_{50}$[a] (nM) | $E_{max}$[b] (%) | Function | Parent cmpds | Dye | $c\log D_{7.4}$[c] |
|---|---|---|---|---|---|---|
| **12** | 82 | 80 | Partial agonist | 1/10b | TAMRA | 3.7 |
| **13** | 528 | 127 | Full agonist | 1/10b | SiR | 3.9 |
| **14** | 77 | 79 | Partial agonist | 1/10b | Alexa488 | −0.5 |
| **15** | 523 | 129 | Full agonist | 1/10b | Alexa467 | −0.9 |
| **16** | 114 | −29 | Inverse agonist | 2/11b | TAMRA | 3.6 |
| **17** | 129 | −29 | Inverse agonist | 2/11b | SiR | 2.2 |
| **18** | 262 | −26 | Inverse agonist | 2/11b | Alexa488 | −0.9 |

[a] The potency ($EC_{50}$ or $IC_{50}$) of fluorescent probes **12–18** was measured using cells stably expressing $hCB_2R$ in homogeneous time-resolved fluorescence (HTRF) cAMP assay. The data are the means of four or seven independent experiments performed in technical replicates. [b] Maximum effect ($E_{max}$ in %) was normalized to reference full agonist **APD371**. [c] For computational calculation of $c\log D_{7.4}$ see ref. 36.

For high probe quality, a lower lipophilicity is crucial, as it significantly reduces non-specific binding.[38] Therefore, it is noteworthy that all predicted $c\log D_{7.4}$ values of our drug-derived probes showed an overall significantly lower lipophilicity compared to phytocannabinoids[21] and are in a favorable drug-like range (Table 2). Moreover, except for highly ionized sulfonated fluorescent dyes such as Alexa488 and Alexa647 (**14**, **15** and **18**), attachment of TAMRA (**12** and **16**) and SiR (**13** and **17**) did not lead to a significant change in the lipophilicity of the final probes compared to their unlabeled counterparts (**10b** $c\log D_{7.4} = 3.8$ and **11b** $c\log D_{7.4} = 3.2$).

### Cellular imaging by flow cytometry and confocal microscopy in live cells

The probe's specificity and suitability for imaging were further validated by flow cytometry. All the fluorescent probes were incubated at various concentrations ranging from 0.014 to 10 μM – with live CHO cells overexpressing $hCB_1R$ or $hCB_2R$ and wild-type (wt) CHO cells as the control. Despite some differences observed in the mean fluorescence intensity (MFI) of probes bearing the same dyes, most of the tested probes indicated decent selectivity and specificity for $hCB_2R$ in flow cytometry, suggesting their suitability for imaging applications.

Probes carrying sulfonated dyes such as Alexa488 **14** and Alexa647 **18** showed high selectivity even at very high concentrations, which is in line with our previous data (ESI, Fig. S-1†).[20] To exclude unspecific binding, we further examined the effect of preincubation of cells with high-affinity competitor ligands such as agonist **JWH133** (ref. 39) and inverse agonist **RO6851228** (ref. 40) on probe **15** binding (ESI, Fig. S-2†). Both ligands competed with **15** in a dose-dependent manner confirming a high target specificity of **15** for $CB_2R$.

Based on the high specificity of the novel probes we continued our investigation by performing time-lapse confocal microscopy experiments to visualize $hCB_2R$ in live CHO cells. Fig. 4 displays the frames of CHO cells overexpressing $hCB_2R$ and $hCB_1R$ along with parental CHO cells 10 min after administration of probes **12**, **14–16** and **18**. All probes selectively stained $CB_2R$ on the cell membrane, but also intracellular staining was observed to some extent, especially for probe **12**. We monitored the staining of **12** in a time-lapse setting and could follow the permeation kinetics through the outer cellular membrane over time, clearly evidencing internalization (ESI, Fig. S-4†). For selected probes, blocking experiments with competitive non-labeled ligands **RO6851228** (ref. 40) ($CB_2R$-inverse agonist) and/or **RO6871304** (ref. 41) ($CB_2R$-agonist) were carried out as well (ESI, Fig. S-3†). Both unlabelled ligands completely blocked the staining of all tested fluorescent probes in $hCB_2R$ expressing CHO cells, confirming the high binding specificity and being fully consistent with the results obtained for WT-CHO and $hCB_1R$ expressing CHO cells.

To further validate the results obtained for CHO cells we continued with imaging human-derived live HEK293 cells expressing $hCB_2R$. We followed the probe **12** distribution in the same manner over 10 min (ESI, Fig. S-5†). Probe **12** exhibited a similar distribution pattern in the human-derived HEK293 cells as in the CHO system, predominantly staining cellular membranes but also the intracellular compartments.

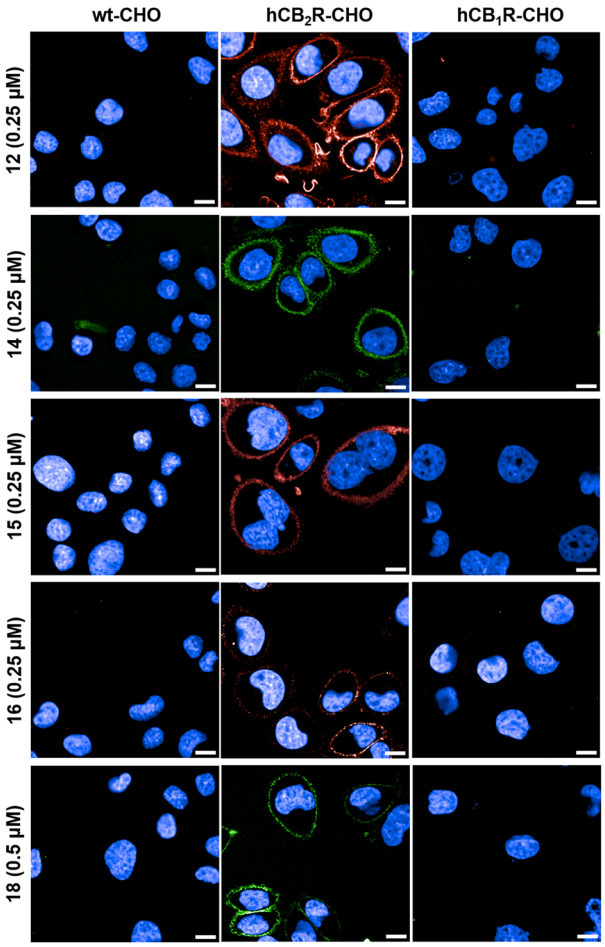


Fig. 4 Time-lapse confocal microscopy in live cells. The wild type (wt) and overexpressing $hCB_2R$- and $hCB_1R$-CHO cells were co-stained with probes **12**, **14–16** and **18** and Hoechst 33342 (blue, nucleus counterstain). The images were recorded 10 min after probe incubation. Images are representative of two independent experiments. Scale bars, 10 μm.

We then set out to visualize endogenous $CB_2R$ expression aiming to ascertain different patterns of activation and localization of $CB_2R$ pools induced by agonist and inverse agonist binding by using non-transfected primary cultures of human macrophages derived from healthy donors. Upon staining of human macrophages with probes **12** and **16** a markedly different distribution pattern was observed (ESI, Fig. S-6†). While agonist probe **12** was widely distributed within the cell, inverse agonist probe **16** was mainly localized on cellular membranes and partially in perinuclear dots, suggesting a distinct localization of inactive and activated $CB_2R$ pools.

### Super-resolution confocal imaging of $hCB_2R$-CHO cells

To examine in more depth the localization and activation states of the $CB_2R$ pools, we resorted to super-resolution confocal imaging of $hCB_2R$ overexpressing CHO cells. First, we assessed the intensity and subcellular distribution of fluorescence

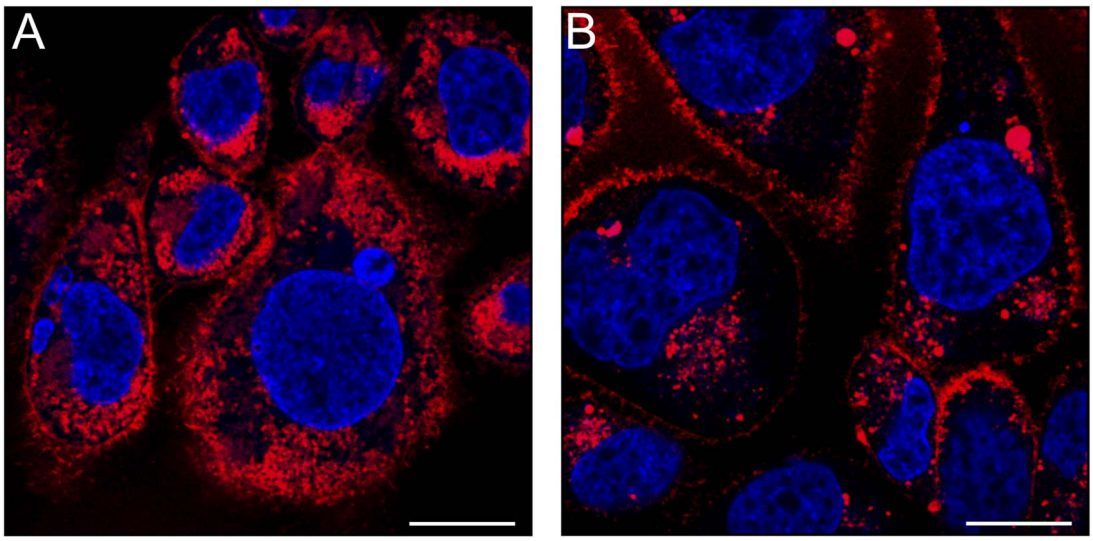


Fig. 5 Super-resolution confocal imaging of overexpressing hCB$_2$R CHO cells. The cells were stained for 15 min with (A) **12** (0.8 μM, red) or (B) **16** (0.8 μM, red) and Hoechst 33342 (blue, nucleus counter stain). Cells were optically sectioned using confocal laser-scanning microscopy equipped with an Airyscan detector. For quantifying the relative levels of labeling using the two TAMRA probes, identical imaging settings (*i.e.*, objective, light path, laser power, gain, offset, frame size, zoom and scan speed) were maintained throughout the acquisition process. Images are representative of three independent experiments. Scale bars, 10 μm.

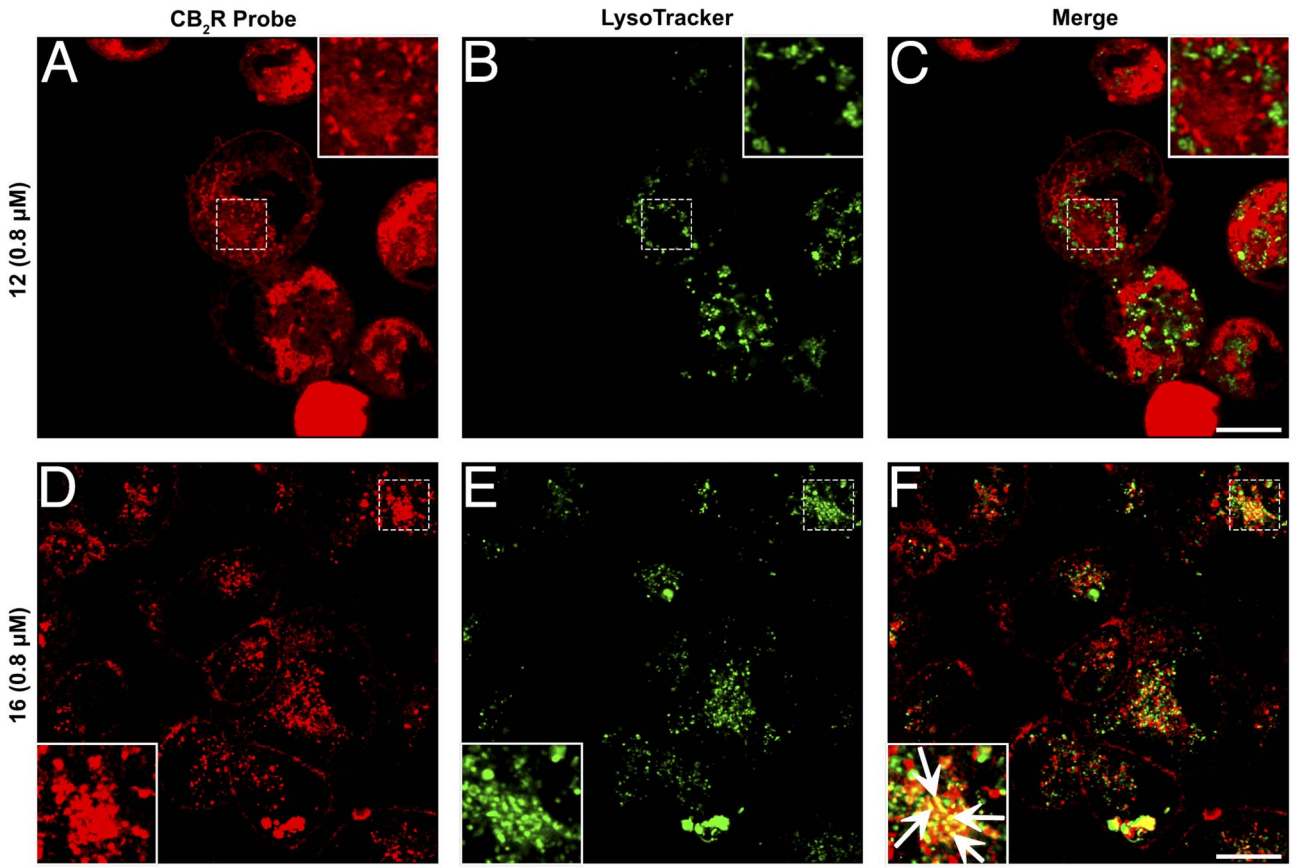


Fig. 6 Co-staining studies utilizing super-resolution confocal microscopy images of hCB$_2$R-CHO cells. (A–F) Double-staining of hCB$_2$R-overexpressing CHO cells exposed for 15 min with **12** (A) or **16** (D) together with LysoTracker, a lysosome marker (B and E, green). Merged images are shown in the panels (C) and (F). The superimposition of the two stainings revealed that **12** and LysoTracker did not colocalize, while **16** and LysoTracker partially co-stained in several dot structures (white arrows in the magnified box). The images are representative of three independent experiments, and in each case, five fields were examined. Scale bars, 10 μm.

staining produced by the matched TAMRA-probe pair **12** and **16**. Image acquisition at higher magnification and resolution was performed after 15 minutes of incubation with **12** and **16** and revealed that both probes yielded a similar localization pattern, yet with distinct labeling intensity. Indeed, for both probes the $CB_2R$ staining was largely observed intracellularly, especially in the perinuclear membranes that are suggestive of the Golgi apparatus and the endoplasmic reticulum; however, appreciable fluorescence was also present on the cell membrane (Fig. 5A and B). Notably, these results corroborate and extend the findings previously reported by den Boon *et al.*[18]

It is noteworthy that the analysis of MFI of **12**-labeled $CB_2R$ showed a plasma membrane labelling intensity of $CB_2R$ approximately six-fold higher than that of **16**-labeled $CB_2R$ (**12**-labeled $CB_2R = 2090 \pm 175$ MFI; **16**-labeled $CB_2R = 350 \pm 4$ MFI; unpaired *t*-test, $t = 19.94$, df $= 4$, and *p*-value $< 0.0001$). Similarly, when examining the intracellular compartments, a marked difference in MFI values was observed (**12**-labeled $CB_2R = 2575 \pm 100$ MFI; **16**-labeled $CB_2R = 340 \pm 13$ MFI; unpaired *t*-test, $t = 37.57$, df $= 4$, and *p*-value $< 0.0001$). This marked difference in labelling intensity still persisted even when differences in binding affinities were compensated for by increasing the concentration of **16** *versus* **12** (ESI, Fig. S-7†). Moreover, comparable quantum yields of probes **12** and **16** in more lipophilic media (ESI, Table S-3†) ruled out potential interference with the observed differences in MFI.

Given that probes **12** and **16** are conjugated with the identical fluorophore and exhibit comparable physicochemical features, including their binding affinity for $CB_2R$, respectively (ESI, Table S-2†), the more pronounced signal detected with probe **12** relative to probe **16** indicates that under steady-state conditions in living cells, $CB_2R$ is present predominantly in its active conformation. It is also plausible that the inactive form of the receptor is less accessible for interaction with probe **16** resulting in weaker labeling when compared to probe **12**.[42,43] We further examined the different distribution patterns of the two probes by co-staining with AlexaFluor488 LysoTracker. Fig. 6 indicates that probe **12** had partial overlap but no clear co-localization with the LysoTracker staining. In contrast, co-staining with probe **16** exhibited a clear co-localization pattern. These results are in line with the observations made on human macrophages (*vide supra*), indicating a distinct intracellular distribution of $CB_2R$ pools, which is influenced by the activation state and may have further implications on cellular signalling pathways. This is consistent with previous extensive studies showing that localization of G protein-coupled receptors (GPCRs) is not restricted to the plasma membrane, but rather is in dynamic exchange with localization in various intracellular compartments, including endosomes, the Golgi apparatus, the endoplasmic reticulum, the nucleus and the mitochondria.[44] This dynamic localization is often influenced by the receptor's activation state, with both active and inactive

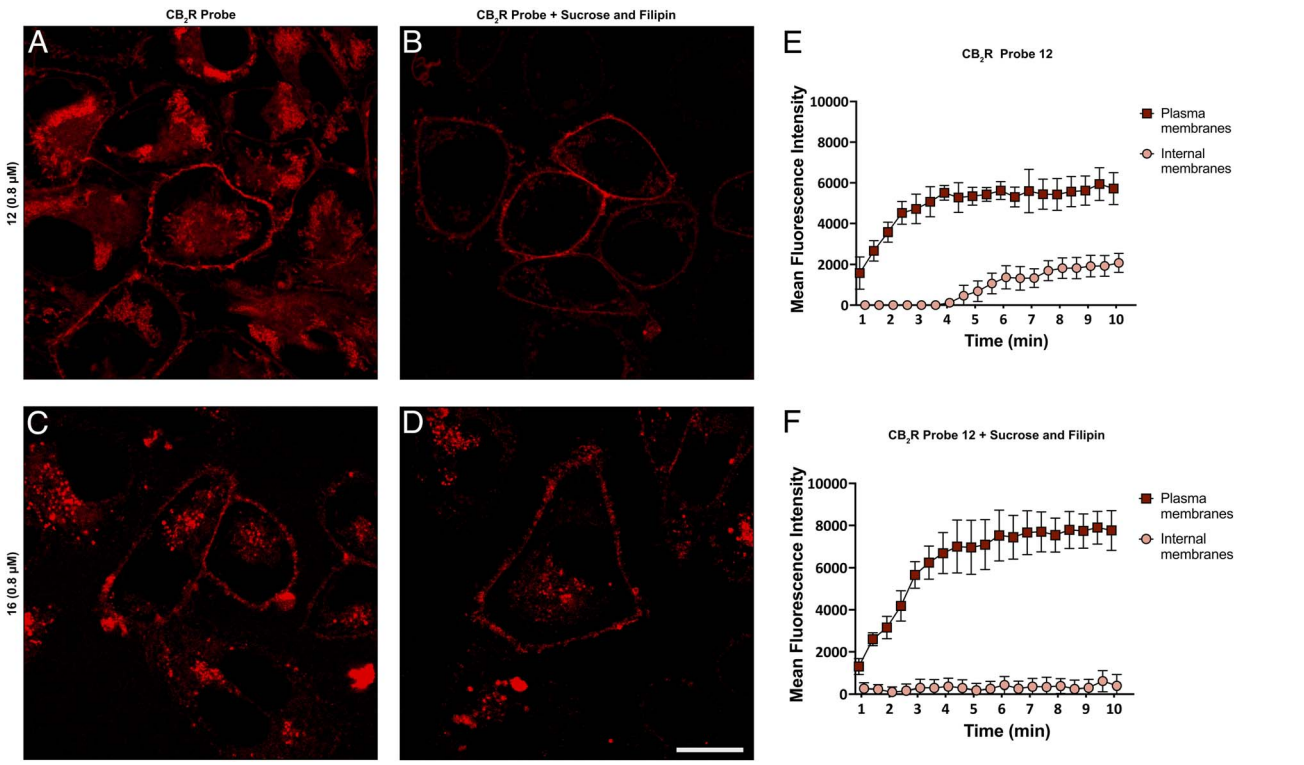


Fig. 7 Endocytosis blocking studies using super-resolution confocal microscopy in $hCB_2R$-CHO cells. Cells were stained for 10 min with **12** (A) or **16** (C). In order to minimize endocytosis, $hCB_2R$-CHO cells were pretreated for 30 min with 400 μM sucrose and 5 μg $mL^{-1}$ filipin and then incubated for 10 min either with **12** (B) or **16** (D). Association curve of **12** on the plasma membrane and internal membranes of $hCB_2R$-CHO cells without sucrose and filipin (E) and in the presence of both (F). Images are representative of three independent experiments. Scale bars, 10 μm. (E) and (F) demonstrate internal and external fluorescence over time.

forms potentially residing within intracellular organelles. $CB_2R$, similar to $CB_1R$, undergoes constitutive endocytosis, resulting in significant intracellular accumulation.[18,45–47] This distribution pattern has been confirmed in leukocytes using anti-$CB_2R$ antibodies.[48] Functionally, $CB_2R$ can be either active or inactive within these subcellular compartments.[17,47] Our findings reveal that inactive $CB_2R$ is presumably partially sequestered in lysosomes and in an as-yet uncharacterized vesicular compartment. We propose that this sequestration may serve as a regulatory mechanism, preventing $CB_2R$ activation and subsequent signalling until the receptor is recycled to the plasma membrane or degraded in the lysosome.

To determine the degree of endocytosis-mediated receptor internalization influenced by the receptor functional state, we performed blocking experiments. Although the experimental setting did not allow for an entire block of endocytosis, a significant reduction was achieved by treating the cells with 0.4 M sucrose and 5 μg $mL^{-1}$ filipin,[21] which can indirectly abrogate multiple pathways of endocytosis.[49] This treatment reduced the intracellular staining of **12** by 70% without affecting that of **16** (see Fig. 7). We recorded the fluorescence intensity of probe **12** by time-lapse imaging and observed signal saturation in both native and blocker-pre-treated cells, both for cytoplasm and internal membranes. In cells pretreated with the endocytotic blockers sucrose and filipin the plasma membrane signal reached the same intensity plateau as in untreated cells, but was negligible for the internal membranes during the entire course of the experiment. The observation that suppression of endocytosis affects the internalization of **12** but does not reduce that of **16** aligns with the behavior of agonists and inverse agonists. Unlike agonists, inverse agonists stabilize the inactive form of a GPCR, which does not promote endocytosis from the membrane.[46,50,51] However, this finding also clearly demonstrates that both probes **12** and **16** are able to reach a significant intracellular concentration by passive permeation in almost the same concentration range. Further investigation into the molecular basis of the differences in localization and activity states might provide valuable insights into the interaction dynamics between $CB_2R$ and its ligands, potentially informing the design of more effective probes or therapeutic agents targeting this receptor.

## Conclusions

In this study, we have developed the first general $CB_2R$ selective matched agonist or inverse agonist platform using validated drug-derived $CB_2R$ ligands **1** and **2**, respectively, as starting points. We designed fluorescent probes sharing highly similar drug-derived chemotypes but addressing either the active or inactive state of $CB_2R$. Due to our reverse-design approach using highly drug-like precursors, all labeled probes exhibited favorable physicochemical properties. The key for the receptor recognition element and fluorophore attachment was a common centrepiece that allowed straightforward linker attachment by amide coupling. The probes retained good binding affinity towards $CB_2R$ and high selectivity against $CB_1R$ upon conjugation of fluorescent dyes. When investigating the functional responses in a cellular cAMP accumulation assay, the labeled probes were able to evoke a similar functional response as their unlabeled congeners. In particular, the labeled inverse agonist enabled us to address the resting state of $CB_2R$. This is of great benefit and importance for various control experiments in live cells which are now possible. With matching TAMRA probes in hand we performed time-lapse confocal microscopy imaging studies in various biological models, including $hCB_2R$-CHO cells, $hCB_2R$-HEK293 cells and human primary macrophages. In all settings, it was clearly demonstrated that $hCB_2R$ has different localization and internalization patterns, depending on the functional state. Most notably, our probes allowed the assessment of localization and distribution of the active and inactive conformations of $CB_2R$ through super-resolution confocal microscopy analysis. These studies indicate that within living cells, a considerable number of $CB_2R$s are located intracellularly and are in an active state. The differential content of the active and inactive states of $CB_2R$ suggests a complex regulatory mechanism governing its activity and interactions with intracellular signalling pathways. These observations, enabled by our matched fluorescent agonist and inverse agonist probe pair, suggest significant implications for understanding the receptor's role in physiological and pathological processes. Furthermore, our approach demonstrates the potential for super-resolution imaging of our $CB_2R$ probes in studying membrane receptors representing a powerful tool for future research in cellular biology and pharmacology.

## Data availability

Primary data for probe synthesis, characterization, photophysical measurements, and fluorescence imaging are provided in the ESI.†

## Author contributions

M. N. and U. G. conceived the research and acquired funding for this project. M. W.-K., A. O., L. M., Y. M., T. G., B. B., W. G., D. V., L. H. H., S. O., M. Ma., U. G., and M. N. designed the research approach. M. W.-K., A. O., L. M., L. S., J. B., X. L., S. R., Y. M., M. S., T. G., C. v. d. H., B. B., A. H., Y. K., W. G., D. S., J. P. v. K., J. Br., T. H., D. V., and S. O. performed experiments, analyzed the raw data, and worked on probe validation. M. W.-K., A. O., L. M., Y. M., S. O., M. Ma., U. G., and M. N. analyzed all data generated and wrote the manuscript. J. B., Y. M., W. G., J. Br., T. H., D. V., and L. H. H. provided useful comments and feedback for the manuscript. All authors have given approval to the final version of the manuscript.

## Conflicts of interest

The authors declare no competing financial interest.

## Acknowledgements

The authors are grateful to Marta Diceglie, Peter Lindemann, Edgar Specker, Katy Franke, Ramona Birke, Andreas Oder,

Astrid Mühl, Peter Schmieder (all Leibniz-Forschungsinstitut für Molekulare Pharmakologie (FMP)), Isabelle Kaufmann, Christian Bartelmus, Oliver Scheidegger, and Claudia Korn (all Roche) for their excellent support in sample handling, analytical compound characterization and helpful discussions. S. O. and M. Ma. thank Dr Franca Abbruzzese (Università Campus Bio-Medico di Roma) for her technical assistance in live cell imaging. This research was partly funded by the European Union – Next Generation EU – NRRP M6C2 – Investment 2.1 Enhancement and strengthening of biomedical research in the NHS (project no. PNRR-MAD-2022-12376730) to S. O. and M. Ma., and EU-OPENSCREEN-DRIVE (Ensuring long-term sustainability of excellence in chemical biology within Europe and beyond) grant no. 823893 to M. N.

## References

1 D. Friedman, J. A. French and M. Maccarrone, Safety, efficacy, and mechanisms of action of cannabinoids in neurological disorders, *Lancet Neurol.*, 2019, **18**, 504.
2 B. S. Basavarajappa, Neuropharmacology of the endocannabinoid signaling system-molecular mechanisms, biological actions and synaptic plasticity, *Curr. Neuropharmacol.*, 2007, **5**, 81.
3 M. Maccarrone, V. D. Marzo, J. Gertsch, U. Grether, A. C. Howlett, T. Hua, A. Makriyannis, D. Piomelli, N. Ueda and M. v. d. Stelt, Goods and Bads of the Endocannabinoid System as a Therapeutic Target: Lessons Learned after 30 Years, *Pharmacol. Rev.*, 2023, **75**, 885.
4 A. C. Howlett and M. E. Abood, in *Adv. Pharmacol.*, ed. D. Kendall and S. P. H. Alexander, Academic Press, 2017, vol. 80, p. 169.
5 H.-C. Lu and K. Mackie, Review of the Endocannabinoid System, *Biol. Psychiatry*, 2021, **6**, 607.
6 R. G. Pertwee, Pharmacology of cannabinoid CB1 and CB2 receptors, *Pharmacol. Ther.*, 1997, **74**, 129.
7 E. Moreno, M. Cavic, A. Krivokuca, V. Casadó and E. Canela, The Endocannabinoid System as a Target in Cancer Diseases: Are We There Yet?, *Front. Pharmacol.*, 2019, **10**, 339.
8 A. Capozzi, V. Mattei, S. Martellucci, V. Manganelli, G. Saccomanni, T. Garofalo, M. Sorice, C. Manera and R. Misasi, Anti-Proliferative Properties and Proapoptotic Function of New CB2 Selective Cannabinoid Receptor Agonist in Jurkat Leukemia Cells, *Int. J. Mol. Sci.*, 2018, **19**, 1958.
9 M. S. García-Gutiérrez and J. Manzanares, Overexpression of CB2 cannabinoid receptors decreased vulnerability to anxiety and impaired anxiolytic action of alprazolam in mice, *J. Psychopharmacol.*, 2010, **25**, 111.
10 P. L. McGeer and E. McGeer, Conquering Alzheimer's Disease by Self Treatment, *J. Alzheimer's Dis.*, 2018, **64**, S361.
11 T. Cassano, S. Calcagnini, L. Pace, F. De Marco, A. Romano and S. Gaetani, Cannabinoid Receptor 2 Signaling in Neurodegenerative Disorders: From Pathogenesis to a Promising Therapeutic Target, *Front. Neurosci.*, 2017, **11**, 30.
12 Z. X. Xi, X. Q. Peng, X. Li, R. Song, H. Y. Zhang, Q. R. Liu, H. J. Yang, G. H. Bi, J. Li and E. L. Gardner, Brain cannabinoid $CB_2$ receptors modulate cocaine's actions in mice, *Nat. Neurosci.*, 2011, **14**, 1160.
13 J. Fernández-Ruiz, J. Romero, G. Velasco, R. M. Tolón, J. A. Ramos and M. Guzmán, Cannabinoid CB2 receptor: a new target for controlling neural cell survival?, *Trends Pharmacol. Sci.*, 2007, **28**, 39.
14 P. Morales, L. Hernandez-Folgado, P. Goya and N. Jagerovic, Cannabinoid receptor 2 (CB2) agonists and antagonists: a patent update, *Expert Opin. Ther. Pat.*, 2016, **26**, 843.
15 W. Bu, H. Ren, Y. Deng, N. Del Mar, N. M. Guley, B. M. Moore, M. G. Honig and A. Reiner, Mild Traumatic Brain Injury Produces Neuron Loss That Can Be Rescued by Modulating Microglial Activation Using a CB2 Receptor Inverse Agonist, *Front. Neurosci.*, 2016, **10**, 1.
16 B. Bie, J. Wu, J. F. Foss and M. Naguib, An overview of the cannabinoid type 2 receptor system and its therapeutic potential, *Curr. Opin. Anaesthesiol.*, 2018, **31**, 407.
17 G. C. Brailoiu, E. Deliu, J. Marcu, N. E. Hoffman, L. Console-Bram, P. Zhao, M. Madesh, M. E. Abood and E. Brailoiu, Differential Activation of Intracellular *versus* Plasmalemmal CB2 Cannabinoid Receptors, *Biochemistry*, 2014, **53**, 4990.
18 F. S. den Boon, P. Chameau, Q. Schaafsma-Zhao, W. van Aken, M. Bari, S. Oddi, C. G. Kruse, M. Maccarrone, W. J. Wadman and T. R. Werkman, Excitability of prefrontal cortical pyramidal neurons is modulated by activation of intracellular type-2 cannabinoid receptors, *Proc. Natl. Acad. Sci. U. S. A.*, 2012, **109**, 3534.
19 J. T. Castaneda, A. Harui and M. D. Roth, Regulation of Cell Surface CB(2) Receptor during Human B Cell Activation and Differentiation, *J. Neuroimmune Pharmacol.*, 2017, **12**, 544.
20 T. Gazzi, B. Brennecke, K. Atz, C. Korn, D. Sykes, G. Forn-Cuni, P. Pfaff, R. C. Sarott, M. V. Westphal, Y. Mostinski, L. Mach, M. Wasinska-Kalwa, M. Weise, B. L. Hoare, T. Miljuš, M. Mexi, N. Roth, E. J. Koers, W. Guba, A. Alker, A. C. Rufer, E. A. Kusznir, S. Huber, C. Raposo, E. A. Zirwes, A. Osterwald, A. Pavlovic, S. Moes, J. Beck, M. Nettekoven, I. Benito-Cuesta, T. Grande, F. Drawnel, G. Widmer, D. Holzer, T. van der Wel, H. Mandhair, M. Honer, J. Fingerle, J. Scheffel, J. Broichhagen, K. Gawrisch, J. Romero, C. J. Hillard, Z. V. Varga, M. van der Stelt, P. Pacher, J. Gertsch, C. Ullmer, P. J. McCormick, S. Oddi, H. P. Spaink, M. Maccarrone, D. B. Veprintsev, E. M. Carreira, U. Grether and M. Nazaré, Detection of cannabinoid receptor type 2 in native cells and zebrafish with a highly potent, cell-permeable fluorescent probe, *Chem. Sci.*, 2022, **13**, 5539.
21 R. C. Sarott, M. V. Westphal, P. Pfaff, C. Korn, D. A. Sykes, T. Gazzi, B. Brennecke, K. Atz, M. Weise, Y. Mostinski, P. Hompluem, E. Koers, T. Miljuš, N. J. Roth, H. Asmelash, M. C. Vong, J. Piovesan, W. Guba, A. C. Rufer, E. A. Kusznir, S. Huber, C. Raposo, E. A. Zirwes, A. Osterwald, A. Pavlovic, S. Moes, J. Beck, I. Benito-Cuesta, T. Grande, S. Ruiz de Martín Esteban, A. Yeliseev, F. Drawnel, G. Widmer, D. Holzer, T. van der Wel,

H. Mandhair, C.-Y. Yuan, W. R. Drobyski, Y. Saroz, N. Grimsey, M. Honer, J. Fingerle, K. Gawrisch, J. Romero, C. J. Hillard, Z. V. Varga, M. van der Stelt, P. Pacher, J. Gertsch, P. J. McCormick, C. Ullmer, S. Oddi, M. Maccarrone, D. B. Veprintsev, M. Nazaré, U. Grether and E. M. Carreira, Development of High-Specificity Fluorescent Probes to Enable Cannabinoid Type 2 Receptor Studies in Living Cells, *J. Am. Chem. Soc.*, 2020, **142**, 16953.

22 F. Spinelli, R. Giampietro, A. Stefanachi, C. Riganti, J. Kopecka, F. S. Abatematteo, F. Leonetti, N. A. Colabufo, G. F. Mangiatordi, O. Nicolotti, M. G. Perrone, J. Brea, M. I. Loza, V. Infantino, C. Abate and M. Contino, Design and synthesis of fluorescent ligands for the detection of cannabinoid type 2 receptor (CB2R), *Eur. J. Med. Chem.*, 2020, **188**, 112037.

23 S. Singh, C. R. M. Oyagawa, C. Macdonald, N. L. Grimsey, M. Glass and A. J. Vernall, Chromenopyrazole-based High Affinity, Selective Fluorescent Ligands for Cannabinoid Type 2 Receptor, *ACS Med. Chem. Lett.*, 2019, **10**, 209.

24 M. Sexton, G. Woodruff, E. A. Horne, Y. H. Lin, G. G. Muccioli, M. Bai, E. Stern, D. J. Bornhop and N. Stella, NIR-mbc94, a fluorescent ligand that binds to endogenous CB(2) receptors and is amenable to high-throughput screening, *Chem. Biol.*, 2011, **18**, 563.

25 L. Scipioni, D. Tortolani, F. Ciaramellano, F. Fanti, T. Gazzi, M. Sergi, M. Nazaré, S. Oddi and M. Maccarrone, Aβ Chronic Exposure Promotes an Activation State of Microglia through Endocannabinoid Signalling Imbalance, *Int. J. Mol. Sci.*, 2023, **24**, 1.

26 C. Bissantz, U. Grether, P. Hebeisen, A. Kimbara, Q. Liu, M. Nettekoven, M. Prunotto, S. Roever, M. Rogers-Evans, T. Schulz-Gasch, C. Ullmer, Z. Wang and W. Yang, *US Pat.*, US20120316147A1, 2012.

27 S. M. Ametamey, K. Atz, L. Gobbi, U. Grether, W. Guba and J. Kretz, WO2020002270A1, 2020.

28 A. Haider, J. Kretz, L. Gobbi, H. Ahmed, K. Atz, M. Bürkler, C. Bartelmus, J. Fingerle, W. Guba, C. Ullmer, M. Honer, I. Knuesel, M. Weber, A. Brink, A. M. Herde, C. Keller, R. Schibli, L. Mu, U. Grether and S. M. Ametamey, Structure–Activity Relationship Studies of Pyridine-Based Ligands and Identification of a Fluorinated Derivative for Positron Emission Tomography Imaging of Cannabinoid Type 2 Receptors, *J. Med. Chem.*, 2019, **62**, 11165.

29 X. Li, H. Chang, J. Bouma, L. V. de Paus, P. Mukhopadhyay, J. Paloczi, M. Mustafa, C. van der Horst, S. S. Kumar, L. Wu, Y. Yu, R. van den Berg, A. P. A. Janssen, A. Lichtman, Z. J. Liu, P. Pacher, M. van der Stelt, L. H. Heitman and T. Hua, Structural basis of selective cannabinoid CB(2) receptor activation, *Nat. Commun.*, 2023, **14**, 1447.

30 R. Slavik, U. Grether, A. Müller Herde, L. Gobbi, J. Fingerle, C. Ullmer, S. D. Krämer, R. Schibli, L. Mu and S. M. Ametamey, Discovery of a High Affinity and Selective Pyridine Analog as a Potential Positron Emission Tomography Imaging Agent for Cannabinoid Type 2 Receptor, *J. Med. Chem.*, 2015, **58**, 4266.

31 A. Haider, L. Gobbi, J. Kretz, C. Ullmer, A. Brink, M. Honer, T. J. Woltering, D. Muri, H. Iding, M. Bürkler, M. Binder, C. Bartelmus, I. Knuesel, P. Pacher, A. M. Herde, F. Spinelli, H. Ahmed, K. Atz, C. Keller, M. Weber, R. Schibli, L. Mu, U. Grether and S. M. Ametamey, Identification and Preclinical Development of a 2,5,6-Trisubstituted Fluorinated Pyridine Derivative as a Radioligand for the Positron Emission Tomography Imaging of Cannabinoid Type 2 Receptors, *J. Med. Chem.*, 2020, **63**, 10287.

32 M. Guberman, M. Kosar, A. Omran, E. M. Carreira, M. Nazaré and U. Grether, Reverse-Design toward Optimized Labeled Chemical Probes – Examples from the Endocannabinoid System, *Chimia*, 2022, **76**, 425.

33 G. Kim, S. J. Weiss and R. L. Levine, Methionine oxidation and reduction in proteins, *Biochim. Biophys. Acta, Gen. Subj.*, 2014, **1840**, 901.

34 L. Mach, A. Omran, J. Bouma, S. Radetzki, D. A. Sykes, W. Guba, X. Li, C. Hoffelmeyer, A. Hentsch, T. Gazzi, Y. Mostinski, M. Wasinska-Kalwa, F. de Molnier, C. van der Horst, J. P. von Kries, M. Vendrell, T. Hua, D. B. Veprintsev, L. H. Heitman, U. Grether and M. Nazare, Highly Selective Drug-Derived Fluorescent Probes for the Cannabinoid Receptor Type 1 (CB(1)R), *J. Med. Chem.*, 2024, **67**, 11841.

35 A. G. Cooper, C. MacDonald, M. Glass, S. Hook, J. D. A. Tyndall and A. J. Vernall, Alkyl indole-based cannabinoid type 2 receptor tools: Exploration of linker and fluorophore attachment, *Eur. J. Med. Chem.*, 2018, **145**, 770.

36 F. Broccatelli, R. Trager, M. Reutlinger, G. Karypis and M. Li, Benchmarking Accuracy and Generalizability of Four Graph Neural Networks Using Large *In Vitro* ADME Datasets from Different Chemical Spaces, *Mol. Inf.*, 2022, **41**, 2100321.

37 S. Bendels, C. Bissantz, B. Fasching, G. Gerebtzoff, W. Guba, M. Kansy, J. Migeon, S. Mohr, J.-U. Peters, F. Tillier, R. Wyler, C. Lerner, C. Kramer, H. Richter and S. Roberts, Safety screening in early drug discovery: an optimized assay panel, *J. Pharmacol. Toxicol. Methods*, 2019, **99**, 106609.

38 M. Honer, L. Gobbi, L. Martarello and R. A. Comley, Radioligand development for molecular imaging of the central nervous system with positron emission tomography, *Drug Discovery Today*, 2014, **19**, 1936.

39 J. W. Huffman, J. Liddle, S. Yu, M. M. Aung, M. E. Abood, J. L. Wiley and B. R. Martin, 3-(1′,1′-Dimethylbutyl)-1-deoxy-Δ8-THC and related compounds: synthesis of selective ligands for the CB2 receptor, *Bioorg. Med. Chem.*, 1999, **7**, 2905.

40 N. Ouali Alami, C. Schurr, F. Olde Heuvel, L. Tang, Q. Li, A. Tasdogan, A. Kimbara, M. Nettekoven, G. Ottaviani, C. Raposo, S. Röver, M. Rogers-Evans, B. Rothenhäusler, C. Ullmer, J. Fingerle, U. Grether, I. Knuesel, T. M. Boeckers, A. Ludolph, T. Wirth, F. Roselli and B. Baumann, NF-κB activation in astrocytes drives a stage-specific beneficial neuroimmunological response in ALS, *EMBO J.*, 2018, **37**, e98697.

41 R. F. Porter, A. M. Szczesniak, J. T. Toguri, S. Gebremeskel, B. Johnston, C. Lehmann, J. Fingerle, B. Rothenhäusler, C. Perret, M. Rogers-Evans, A. Kimbara, M. Nettekoven, W. Guba, U. Grether, C. Ullmer and M. E. M. Kelly, Selective Cannabinoid 2 Receptor Agonists as Potential Therapeutic Drugs for the Treatment of Endotoxin-Induced Uveitis, *Molecules*, 2019, **24**, 1.

42 X. Li, T. Hua, K. Vemuri, J.-H. Ho, Y. Wu, L. Wu, P. Popov, O. Benchama, N. Zvonok, K. a. Locke, L. Qu, G. W. Han, M. R. Iyer, R. Cinar, N. J. Coffey, J. Wang, M. Wu, V. Katritch, S. Zhao, G. Kunos, L. M. Bohn, A. Makriyannis, R. C. Stevens and Z.-J. Liu, Crystal Structure of the Human Cannabinoid Receptor CB2, *Cell*, 2019, **176**, 459.

43 C. Xing, Y. Zhuang, T.-H. Xu, Z. Feng, X. E. Zhou, M. Chen, L. Wang, X. Meng, Y. Xue, J. Wang, H. Liu, T. F. McGuire, G. Zhao, K. Melcher, C. Zhang, H. E. Xu and X.-Q. Xie, Cryo-EM Structure of the Human Cannabinoid Receptor CB2-Gi Signaling Complex, *Cell*, 2020, **180**, 645.

44 I. Fasciani, M. Carli, F. Petragnano, F. Colaianni, G. Aloisi, R. Maggio, M. Scarselli and M. Rossi, GPCRs in Intracellular Compartments: New Targets for Drug Discovery, *Biomolecules*, 2022, **12**, 1343.

45 C. Leterrier, D. Bonnard, D. Carrel, J. Rossier and Z. Lenkei, Constitutive endocytic cycle of the CB1 cannabinoid receptor, *J. Biol. Chem.*, 2004, **279**, 36013.

46 C. Leterrier, J. Laine, M. Darmon, H. Boudin, J. Rossier and Z. Lenkei, Constitutive activation drives compartment-selective endocytosis and axonal targeting of type 1 cannabinoid receptors, *J. Neurosci.*, 2006, **26**, 3141.

47 G. Salort, M. Alvaro-Bartolome and J. A. Garcia-Sevilla, Regulation of cannabinoid CB(2) receptor constitutive activity in vivo: repeated treatments with inverse agonists reverse the acute activation of JNK and associated apoptotic signaling in mouse brain, *Psychopharmacology*, 2017, **234**, 925.

48 J. T. Castaneda, A. Harui, S. M. Kiertscher, J. D. Roth and M. D. Roth, Differential expression of intracellular and extracellular CB(2) cannabinoid receptor protein by human peripheral blood leukocytes, *J. Neuroimmune Pharmacol.*, 2013, **8**, 323.

49 K. M. Kitchens, R. B. Kolhatkar, P. W. Swaan and H. Ghandehari, Endocytosis inhibitors prevent poly(amidoamine) dendrimer internalization and permeability across Caco-2 cells, *Mol. Pharm.*, 2008, **5**, 364.

50 C. Oliveira de Souza, X. Sun and D. Oh, Metabolic Functions of G Protein-Coupled Receptors and beta-Arrestin-Mediated Signaling Pathways in the Pathophysiology of Type 2 Diabetes and Obesity, *Front. Endocrinol.*, 2021, **12**, 715877.

51 C. Parnot, S. Miserey-Lenkei, S. Bardin, P. Corvol and E. Clauser, Lessons from constitutively active mutants of G protein-coupled receptors, *Trends Endocrinol. Metab.*, 2002, **13**, 336.